

# Self-Supervised Visual Place Recognition by Mining Temporal and Feature Neighborhoods

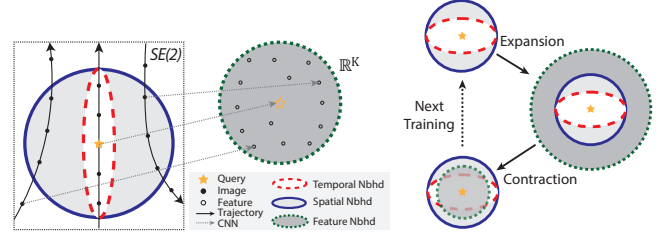
Chao Chen<sup>1</sup>, Xinhao Liu<sup>1</sup>, Xuchu Xu<sup>1</sup>, Yiming Li<sup>1</sup>, Li Ding<sup>2</sup>, Ruoyu Wang<sup>1</sup>, and Chen Feng<sup>✉,1</sup>

**Abstract**—Visual place recognition (VPR) using deep networks has achieved state-of-the-art performance. However, most of them require a training set with ground truth sensor poses to obtain positive and negative samples of each observation’s spatial neighborhood for supervised learning. When such information is unavailable, temporal neighborhoods from a sequentially collected data stream could be exploited for self-supervised training, although we find its performance suboptimal. Inspired by noisy label learning, we propose a novel self-supervised framework named *TF-VPR* that uses temporal neighborhoods and learnable feature neighborhoods to discover unknown spatial neighborhoods. Our method follows an iterative training paradigm which alternates between: (1) representation learning with data augmentation, (2) positive set expansion to include the current feature space neighbors, and (3) positive set contraction via geometric verification. We conduct comprehensive experiments on both simulated and real datasets, with either RGB images or point clouds as inputs. The results show that our method outperforms our baselines in recall rate, robustness, and heading diversity, a novel metric we propose for VPR. Our code and datasets can be found at <https://ai4ce.github.io/TF-VPR/>.

## I. INTRODUCTION

Visual place recognition (VPR), which aims to identify previously visited places based on current visual observation, is a well-known problem in computer vision and plays a crucial role in autonomous robots [1]. Meanwhile, VPR is closely related to re-localization [2], loop closure detection [3], and image retrieval [4]. Despite all the efforts, VPR remains a difficult task due to various challenges such as perceptual aliasing and view direction differences [5], [6]. Classic VPR methods based on hand-crafted feature matching do not require supervised learning, but are less robust to the challenges mentioned above [7]–[9]. Therefore, learning-based methods have been proposed to learn local or global feature descriptors [10] by place classification [11] or contrastive-like similarity learning [12]. Some works also use a short image sequence instead of a single image to mitigate the issue of perceptual aliasing [13]–[15].

So far, most learning-based VPR methods are supervised, focusing on either learning better feature representations or designing robust matching strategies. They assume that accurate positions (and sometimes orientations) are available in their training set, for obtaining the positive and negative



(a) A partial sensory stream & 3 types of neighbors (red/blue/green circles). (b) A spatial neighborhood’s iterative update.

Fig. 1: **Our idea** is based on the interconnections between the **temporal**, **spatial**, and **feature** neighborhoods in sensory data: a query’s spatial neighborhood expands from its temporal to feature neighbors, then contracts to exclude wrong neighbors, iterated in training until such neighborhoods’ convergence.

neighbors of each visual observation [10], [12], or defining place categories [11]. However, this information could be onerous to obtain due to GPS errors and its indoor unavailability or SLAM robustness challenges, especially at a large scale. Considering human’s extraordinary VPR ability that does not seem to need ground truth pose information for its training, we ask the following question: *is it possible to relax such an assumption and design a learning-based VPR approach without pose-dependent supervision?*

To achieve this goal, our main idea is to *leverage fixed temporal neighborhoods and learnable feature neighborhoods to discover the unknown spatial neighborhoods* (which require ground truth pose to compute), leading to a self-supervised VPR method shown in Fig. 1. We are inspired by research work utilizing sensory streams (RGB videos or point cloud sequences) to obtain the positive and negative neighbors in the temporal domain such as [16]. However, we find that VPR learned from temporal cues alone will miss spatial neighboring places with large viewpoint differences, because temporal neighbors tend to share similar viewpoints.

This is suboptimal in applications such as visual navigation or loop closure for SLAM. To automatically discover the true spatial neighbors with diverse viewpoints, we propose a novel iterative learning strategy inspired by noisy label training such as bootstrapping [17]. More specifically, we exploit the temporal information for label initialization as shown in Fig. 1a. We further augment the labels by simulating observations perceived from different view directions. Afterward, a feature representation will be learned based on the current labels. Finally, as shown in Fig. 1b, we re-label the dataset using the learned feature space by: (1) adding

✉ Corresponding author.

<sup>1</sup>Chao Chen, Xinhao Liu, Xuchu Xu, Yiming Li, Ruoyu Wang, and Chen Feng are with New York University, Brooklyn, NY 11201, USA [cfeng@nyu.edu](mailto:cfeng@nyu.edu)

<sup>2</sup>Li Ding is with University of Rochester, Rochester, NY 14627, USA [l.ding@rochester.edu](mailto:l.ding@rochester.edu)

feature-space neighbors as tentative positive labels and (2) rejecting false positives via geometric verification, in order to further refine the feature representation. Note that the above steps are iteratively conducted until convergence.

To evaluate our self-supervised VPR with Temporal and Feature neighborhood interactions (**TF-VPR**), we simulate datasets with different input modalities, and develop a real-world dataset NYU-VPR-360 including two scenes with 38,426 GPS-georeferenced images in total. All the datasets are sequentially-collected sensory streams. Meanwhile, we develop a novel metric to measure the heading diversity of the retrieval results. In summary, our contributions are:

- 1) We propose a novel self-supervised VPR solution termed TF-VPR that eliminates pose-dependent supervision by mining temporal and feature neighborhoods.
- 2) We propose a new evaluation metric to assess the heading diversity of VPR retrieval results.
- 3) We conduct comprehensive experiments in both simulation and real-world to demonstrate the advantages of our solution compared with other baseline methods. Our codes and data will be released with this paper.

## II. RELATED WORK

**Visual place recognition.** Visual place recognition (VPR) is the problem of identifying a previously visited place based on visual information [5]. Existing VPR methods mainly lie in two categories: (1) traditional VPR techniques using hand-crafted features [18]–[23], and (2) state-of-the-art VPR techniques using deep learning [12], [24]–[27]. Among those, NetVLAD [12] is a seminal deep-learning-based VPR framework, followed by various research extensions such as (1) learning powerful feature representation [28], [29], (2) designing robust matching strategies [13]–[15], and (3) investigating different input modalities in VPR [30]–[33]. However, most methods are supervised by pose-dependent data [12], [24]–[26]. To relax such a constraint, several attempts have been made [34]–[37], yet failed to handle diverse re-visiting viewpoints. The most relevant work to our method is the semi-parametric topological memory (SPTM) [16], which utilizes temporal positives and negatives to train a binary classification network for adding edges for topological mapping, similar to VPR. However, since temporal neighbors tend to have very similar viewpoints, SPTM still struggles to recognize revisits of the same place from different viewpoints. To the best of our knowledge, no research has addressed *self-supervised VPR* that can recognize places observed from *various viewpoints* as *either 2D images or 3D point clouds*.

**Noisy label learning.** Noisy labels become a problem as training data size increases, resulting in degraded performance [38]. To mitigate the issues of noisy labels, several learning attempts [39] have been made from directions including latent variable optimization [40], loss function design [41], and pseudo-label-based self-training [17], [42]–[44]. Among all pseudo-label methods, label refurbishment was firstly introduced by Bootstrapping [17]. Later on,

another method addressed this problem using a self-training-based approach with an iterative workflow [43] which was used as a baseline architecture in their more recent framework confidence regularized [44]. Our method’s iterative training paradigm takes inspiration from [43], [44].

**Contrastive learning.** It is a self-supervised learning technique to find feature representations that differentiate similar data pairs from dissimilar ones without labels. Data augmentation is often used, and the learning objective is to decrease feature distances between the original and augmented images (positive samples), while increasing those distances between different images (negative samples) [45]–[48]. In VPR, NetVLAD [30] uses the triplet loss which is similar to contrastive learning, yet relies on ground truth pose to define positive/negative samples. Building on NetVLAD, we further adopt data augmentation to synthesize observations captured by different viewpoints in order to learn more robust features for VPR.

**VPR evaluation.** There are several evaluation metrics for visual place recognition, *e.g.*, the popular AUC-PR [1] provides a good overview of precision and recall performance but is less indicative in the cases when ground truth match could take multiple values. Recall Rate@N, as used in [12], [49], [50], is designed to address such cases that the correct retrieval may be in the top-N results, and multiple correct query matches are neither penalized nor rewarded. However, existing VPR metrics rarely evaluate the viewpoint diversity of the retrieved results [5], which is important in downstream applications such as SLAM. In this work, we develop such a metric to fill this gap. It assesses a VPR model’s capacity to recognize places revisited from different directions.

## III. METHODOLOGY

We focus on a robot that is collecting a sensory stream of surround-view visual observations while navigating in a certain area. Our goal is to enable the robot to achieve visual place recognition (VPR) in the same spatial area where the data stream is collected, without relying on any frame-wise pose information. To this end, we utilize a learnable neural network  $f_\theta$  parameterized by  $\theta$  to map each visual observation to discriminative feature space for VPR. However, it is non-trivial to train such a neural network without ground-truth labels. In this work, we propose a novel iterative learning paradigm based on the following intuition: for the  $i$ -th query observation  $\mathbf{q}_i$ , its spatial positive set  $\mathcal{P}_{\mathbf{q}_i}$  could be inferred by its temporal positive set  $\mathcal{P}_{\mathbf{q}_i}^t$  together with its tentative feature-space positive set  $\mathcal{P}_{\mathbf{q}_i}^f$ .

**Our objective: auto-labeling with self-supervised learning.** Different from existing supervised VPR methods that need to address the generalizability of learned models, we aim to solve VPR only for a certain spatial area where the data has been collected. Given an observation sequence, we want to automatically label each data frame’s spatial topology without ground truth poses for supervision. Similar to DeepMapping [51], we do not expect the learned  $f_\theta$  to generalize its VPR ability either to *other areas* or to *the same area but under different times/seasons/weather conditions*



$\{\mathbf{o}_k\}_{k=1}^K$ . Then we utilize the maximum feature distance between the query and its temporal neighbors as a frame-specific threshold  $\tau_i$  to determine which candidates should be included in the expanded positive set:

$$\tau_i = \max_{\mathbf{p}_j \in \mathcal{P}_{\mathbf{q}_i}^t} d(\mathbf{q}_i, \mathbf{p}_j), \quad (2)$$

where  $\mathcal{P}_{\mathbf{q}_i}^t$  is the temporal neighborhood set for query  $\mathbf{q}_i$ ,  $i$  and  $j$  are the frame indices. Finally, any candidate  $\mathbf{o}_k$  (selected from KNN) with a smaller feature distance to the query than the threshold  $\tau_i$  will form the feature neighborhood set:  $\mathcal{P}_{\mathbf{q}_i}^f = \{\mathbf{o}_k\}_{d(\mathbf{q}_i, \mathbf{o}_k) < \tau_i}$ .

#### E. Contraction

To avoid potential false positives caused by noisy feature space during learning, we employ geometric verification to check the validity of feature neighborhoods  $\mathcal{P}_{\mathbf{q}_i}^f$  before using it to update  $\mathcal{P}_{\mathbf{q}_i}^{(e)}$ . We adopt different distance measures (independent of the neural network) based on input modality: the number of matching points for images [52] and the Chamfer distance after ICP for point clouds [53]. The verification strategy is similar to the one for KNN feature neighborhoods verification: we consider the maximum distance between the query and its temporal neighborhoods as the threshold. Then any candidate with a distance value within the threshold will pass the verification. The verified feature neighborhoods denoted by  $\hat{\mathcal{P}}_{\mathbf{q}_i}^f$  are permanently added into the positive set:

$$\mathcal{P}_{\mathbf{q}_i}^{(e+1)} = \mathcal{P}_{\mathbf{q}_i}^{(e)} \cup \hat{\mathcal{P}}_{\mathbf{q}_i}^f, \quad (3)$$

where  $e$  is the number of learning epochs. Note that  $\mathcal{N}_{\mathbf{q}_i}^{(e)}$  will also be updated similarly. Afterward, the model will be trained with the updated labels until convergence.

### IV. EXPERIMENTS

We test TF-VPR in three different kinds of environments: simulated 2D point clouds [51], simulated RGB images [54], and real-world RGB images. Our codebase uses PyTorch [55] with network parameters optimized using Adam [56]. The learning rate is tuned to 0.001. We compare TF-VPR with both supervised and self-supervised baseline methods.

#### A. Evaluation metrics

**Recall rate (Recall@N)** is the ratio of successful retrievals to a total number of queries, where a successful retrieval means at least one of the top-N retrieved results is also the ground-truth spatial neighbor of the query. Ground truth can be obtained by K-D tree search on geographical location  $(x, y, z)$  within a certain radius  $R$ . Note that when computing this metric, we need to exclude the temporal neighbors of a query from its top-N retrievals. This is because in our auto-labeling setup, the temporal-based methods can easily overfit the temporal neighborhood, leading to uninformative evaluation with recall rates that are always close to 100% if the temporal neighbors are kept in ground truth.

**Heading diversity (HD)** measures the diversity of sensor headings of the true positives (w.r.t. the query's heading)

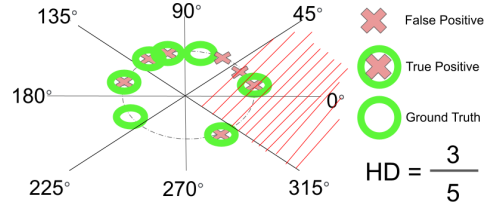


Fig. 3: **Heading diversity illustration.** The angle represents the heading difference between the query and the evaluated positives. HD represents how many angular bins are covered by true positives vs. that by the ground truth. The figure gives an example of how to calculate HD. Excluding the first and last bins,  $\mathcal{P}_{\mathbf{q}_i}^f$  contains 5 retrieved non-temporal positives, 4 of which are true positives, and they fall into 3 different bins, while ground truth covers 5 bins, so HD is  $3/5$  (not  $4/5$ ).

among the top- $|GT|$  retrievals.  $|GT|$  is the size of ground-truth set that can be obtained based on a specific radius  $R$  as described in Recall@N. First, we believe that those positives with headings different than the query are more valuable in downstream applications. Thus, we evenly divide the  $360^\circ$  range of headings into 8 angular bins in our setup, ignoring the first and last bins because they contain positives with similar headings w.r.t. the query. In this case, the  $m$ -th bin covers the heading difference range  $\mathcal{Q}_m$  as:

$$\mathcal{Q}_m = [m \times 45^\circ, (m+1) \times 45^\circ], m \in [1, 2, 3, 4, 5, 6]. \quad (4)$$

Then, we define HD for a query  $\mathbf{q}$  as the bin coverage ratio between the true positives and the ground truth:

$$\text{HD}(\mathbf{q}) = \frac{\sum_{m \in [1 \dots 6]} \mathbb{1}(\exists \mathbf{x} \in \tilde{\mathcal{P}}_{\mathbf{q}}^{GT} \wedge (\theta_{\mathbf{q}} - \theta_{\mathbf{x}}) \in \mathcal{Q}_m)}{\varepsilon + \sum_{m \in [1 \dots 6]} \mathbb{1}(\exists \mathbf{y} \in \mathcal{P}_{\mathbf{q}}^{GT} \wedge (\theta_{\mathbf{q}} - \theta_{\mathbf{y}}) \in \mathcal{Q}_m)}, \quad (5)$$

where  $\theta_{\mathbf{q}}$  and  $\theta_{\mathbf{x}}$  are respectively the heading of the query and a frame  $\mathbf{x}$ ,  $\tilde{\mathcal{P}}_{\mathbf{q}}^{GT}$  is the set of true positives in the top- $|GT|$  retrievals,  $\mathcal{P}_{\mathbf{q}}^{GT}$  is the ground truth positive set,  $\varepsilon$  is an arbitrarily small positive quantity to avoid zero division error, and  $\mathbb{1}(\cdot)$  is the indicator function. See Fig. 3 for an example. Finally, we report the averaged HD for all queries.

#### B. Experiments on simulated point cloud dataset

**Dataset.** We generate the 2D point cloud dataset using the tool provided in [51]. Specifically, we create a large environment as a  $1024 \times 1024$  binary image in which black and white pixels respectively represent the occupied and free-space locations in the 2D environment. We then manually generate a set of trajectories in this environment, each of which contains a sequence of 2048 poses. At each pose, a point cloud scan is simulated by finding the intersection points between 2D LiDAR rays and occupied space in the environment. The simulated 2D point cloud dataset contains 3 different environments and 18 trajectories in each environment. Each scan contains 256 points.

**Baseline methods.** We compare TF-VPR with the following baselines: (1) PointNetVLAD [30] trained with pose-based supervision, (2) PointNetVLAD trained with temporal pseudo labels as in [16] (SPTM), (3) SPTM with data



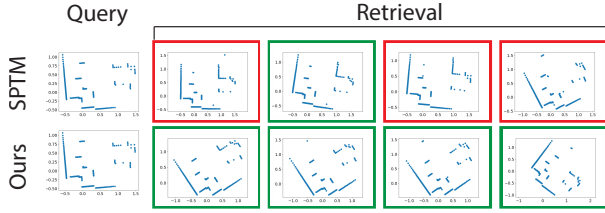


Fig. 4: **Qualitative VPR results on 2D point cloud dataset.** The first row shows the results of SPTM [16] and the second row shows the results of **TF-VPR**. The first column is the query point cloud and column 2-5 are the top 4 retrievals. **Green** and **red** respectively indicate true and false positives.

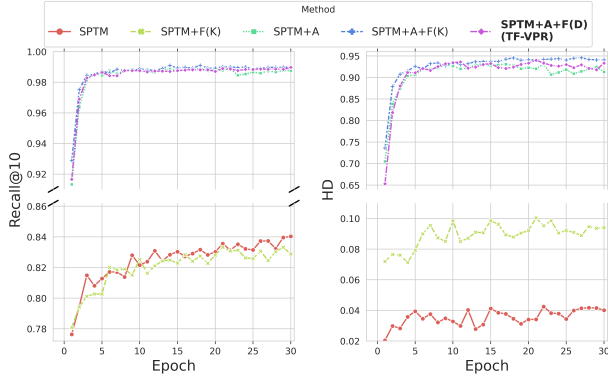


Fig. 5: **Recall@10 and HD with respect to training epoch** on 2D point cloud dataset.  $F$  denotes method with feature neighborhoods,  $A$  denotes method with data augmentation,  $(K)$  denotes method with KNN during expansion,  $(D)$  denotes method with dynamic KNN in expansion.

augmentation (SPTM+A), (4) SPTM with feature-neighbor KNN expansion (SPTM+F(K)), and (5) SPTM+A+F(K). Note that the contraction step is not used for this simulated toy dataset, because we found the expansions are all correct in this case.

**Implementation details.** The network architecture for the SPTM baseline is the same as PointNetVLAD. We select  $n = 5$  and  $u = 2$  in Section III-B. The value of  $n$  depends on the sampling rate of the sensor. Additionally, similar to the training in [30], we randomly select only 2 positives and 18 negatives to speed up the loss computation. The output feature dimension is 512. Based on the sampling rate of the sensor, for each query, we exclude its closest 10 temporal neighbors from the top- $N$  retrievals as explained in IV-A.

**Data augmentation.** Fig. 5 shows a significant improvement in both recall@10 and HD after augmentation is added to SPTM. SPTM fails to retrieve the true neighbors from different headings, leading to insufficient retrievals. Differently, SPTM+A uses augmented positives in the triplet loss, leading to a network that is insensitive to the orientation of the point cloud inputs. Thus, in Fig. 4, with augmentation, TF-VPR demonstrates its capability to retrieve positives from diverse directions.

**Feature-neighbor expansion.** SPTM+F(K) has slightly poorer performance than the original SPTM as shown in Fig. 5, because only adding positives from the same direction

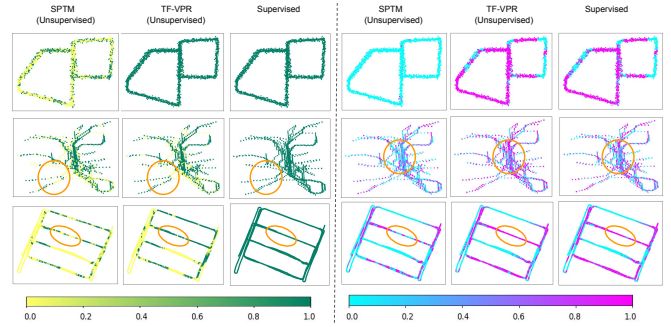


Fig. 6: **Per-frame performance visualization** over ground truth trajectories on point cloud (top), simulated RGB (middle), and NYU-VPR-360 (bottom) datasets. The left block shows the Recall@10 and the right block shows the HD metrics. Each query’s metrics at epoch 30 are color-coded.

TABLE I  
QUANTITATIVE RESULTS ON 2D SIMULATED POINT CLOUD DATA. WE EMPLOY BEST RECALL RATE (R) AND HEADING DIVERSITY (HD).

Method / Metric	R@10	R@5	R@1	HD
SPTM [16]	93.36	91.06	79.10	4.25
<b>TF-VPR (Ours)</b>	<b>99.71</b>	<b>99.66</b>	<b>98.73</b>	<b>93.62</b>
PointNetVLAD [30]	100.00	100.00	100.00	89.38

does not provide extra valuable training data. In comparison, SPTM with data augmentation and feature space neighborhood (SPTM+A+F(K)) helps feature-neighbor expansion more effectively discover true neighbors from different headings, thereby improving performance.

**Dynamic KNN.** We further study the effectiveness of dynamic KNN compared to fixed KNN in TF-VPR, i.e., SPTM+A+F(D) vs. SPTM+A+F(K). The difference is negligible on the simulated point cloud dataset. However, the difference would be larger on NYU-VPR-360 dataset.

**Performance difference between TF-VPR and other baselines.** In Table I, among all of these methods, TF-VPR shows a comparable result of recall rate and heading diversity to PointNetVLAD, and outperforms SPTM by a large margin. Moreover, Fig. 6 visualizes the per-frame retrieval quality over the datasets’ ground truth trajectories, and SPTM clearly performs the worst with more failures.

### C. Experiments on photorealistic RGB dataset

**Dataset.** TF-VPR has also been tested via habitat-sim [54] simulator on the Gibson photorealistic RGB dataset [58], which provides panoramic RGB images for a variety of indoor scans. We capture RGB images by a panoramic camera mounted on a robot moving randomly in the virtual environment. We captured a total of 33,679 RGB images in three Gibson rooms. Each image is downsampled to  $256 \times 64$  pixels. In contrast to other datasets, this simulated RGB dataset contains a large number of revisits of places from both similar and different directions, which is useful for testing recall rate and heading diversity for VPR.

**Baseline methods.** The following baselines are evaluated: (1) NetVLAD [12] trained with pose-based supervision, (2) NetVLAD trained with temporal pseudo labels as in [16] (SPTM), (3) prototypical contrastive learning (PCL) [57] as

TABLE II

QUANTITATIVE RESULTS ON PHOTOREALISTIC RGB DATA. WE EMPLOY BEST RECALL RATE (R) AND HEADING DIVERSITY (HD). WE REPORT RESULTS ON THREE ROOMS IN HABITAT-SIM (GOFFS, MICANOPY, AND SPOTSWOOD).

Scene	Goff's				Micanopy				Spotswood			
Metric	R@10	R@5	R@1	HD	R@10	R@5	R@1	HD	R@10	R@5	R@1	HD
SPTM [16]	95.52	94.69	90.15	55.28	95.13	94.32	90.06	56.37	96.33	95.65	92.16	54.41
SPTM (epoch 30) [16]	94.50	93.28	88.03	49.61	92.89	90.20	78.27	50.47	93.53	91.23	81.52	49.69
PCL [57]	49.27	42.86	27.00	0.35	60.36	54.18	37.73	0.19	57.36	51.66	35.33	0.03
VLAD [8], [9]	42.48	30.69	12.54	0.07	49.23	37.82	17.36	0.00	53.52	41.23	16.53	0.12
TF-VPR (Ours)	<b>96.31</b>	<b>96.00</b>	<b>93.62</b>	<b>67.67</b>	<b>95.59</b>	<b>95.21</b>	<b>93.42</b>	<b>65.97</b>	<b>96.91</b>	<b>96.57</b>	<b>95.35</b>	<b>69.39</b>
TF-VPR (Ours) (epoch 30)	96.15	95.82	93.31	66.54	95.46	94.93	92.82	63.94	96.66	96.32	94.66	65.59
NetVLAD [12]	99.63	99.16	96.36	60.48	99.48	99.26	97.38	63.38	99.56	99.17	96.60	64.64

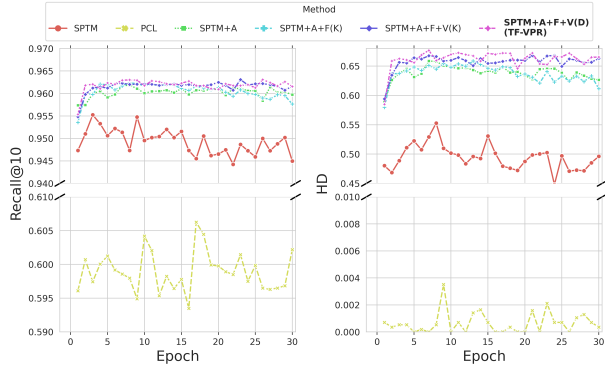


Fig. 7: **Recall@10 and HD vs. training epoch** on the photorealistic dataset (Goff's).  $V$  denotes method with geometric verification. Other abbreviations follow Fig. 5.

another self-supervised VPR method used in visual navigation [37], (4) VLAD [8], [9] as a classic non-deep-learning VPR, and the previous ablation study baselines.

**Implementation details.** To speed up computation, the output dimension is set to 512. Our implementation is based on the code from NetVLAD. The method for converting NetVLAD to SPTM is similar to Section IV-B. Similarly, we also choose  $n = 5$  and  $u = 2$  in Section III-B, and exclude for each query's closest 30 temporal neighbors from the top- $N$  retrievals as explained in IV-A.

Considering new baselines involved, PCL is implemented as the default setting. We need to tune the total number of clusters. In this experiment, we tried to set the total number of clutter to 200, 500, and 1000 and select the best result. For the VLAD baseline, we use the classic 128-dimensional SIFT features, and a cluster size of 32. The raw VLAD descriptor dimension of  $32 \times 128$  is further reduced to 512 by PCA.

**Importance of contraction.** Geometric verification becomes more important for RGB data. The generated positive candidate is not as trustworthy as in the toy dataset in Section IV-B. As a result, including geometric verification helps maintain or even increase accuracy. From Fig. 7, we can observe that both metrics in all methods other than TF-VPR decline with respect to training epochs, because they overfit temporal neighbors as depicted in the first stage in Fig. 1b. And they tend to miss true spatial neighbors. To prevent this, the feature space neighborhood together with the verification discovers more reliable positives in  $\hat{\mathcal{P}}_{q_i}^f$  to be added into  $\mathcal{P}_{q_i}$ , as depicted in the third stage of Fig. 1b. The stability of the model performance over training epochs is

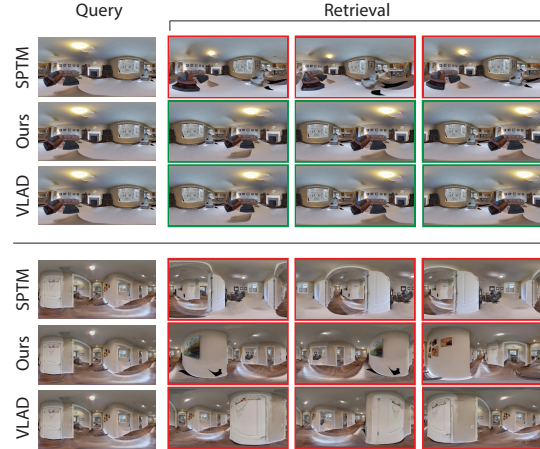


Fig. 8: **Qualitative VPR results on the photorealistic RGB dataset.** The upper part shows an example where **TF-VPR** outperforms SPTM [16], and the lower part depicts a challenging example in which none of the methods retrieve the data correctly. **Green** and **red** indicates true and false non-temporal spatial positives, respectively. Although the frames in the first row appear to be positives, their positions are still far from the query. Due to the high frame density in the habitat-sim dataset, frames can only be considered positives if they are no more than 20cm apart from the query.

critical for self-supervised VPR in reality because we would not know when to stop training without ground truth poses.

**Ablation study on habitat-sim.** As shown in Fig. 7 and Table II, TF-VPR outperforms all unsupervised baselines, and approaches the supervised NetVLAD performance in both recall rate and heading diversity (HD). Particularly, HD is improved by a large margin, particularly for scenes with a high number of revisits from different directions. On average, TF-VPR improves recall rate by 1% and heading diversity by 10%. Fig. 6 visualizes the retrieval quality on the simulated RGB dataset. SPTM can make reasonably accurate estimates in recall@10 and HD. TF-VPR outperforms SPTM, but the improvement is not significant. Especially, the improvement of HD in the RGB dataset is not comparable to that in the point cloud dataset, because RGB images appear to be less resistant to environmental changes such as lighting and seasons. The qualitative results are in Fig. 8.

**PCL, VLAD, and conventional visual SLAM system.** Table II shows the poor performance of PCL and VLAD. We believe that PCL might not be a good VPR solution, because most contrastive learning methods do form several disjoint

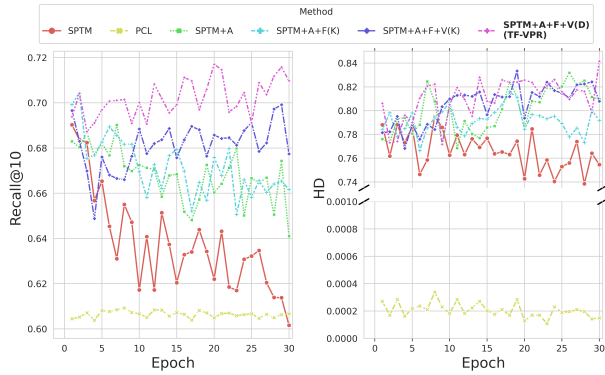


Fig. 9: Recall@10 and HD vs. training epoch on NYU-VPR-360 (scene 1). Abbreviations follow Fig. 7.

TABLE III

QUANTITATIVE RESULTS ON NYU-VPR-360 DATASET. WE EMPLOY BEST RECALL RATE (R) AND HEADING DIVERSITY (HD). TWO SCENES HAVE BEEN REPORTED (SCENE1, SCENE2).

Scene	Scene 1				Scene 2			
	R@10	R@5	R@1	HD	R@10	R@5	R@1	HD
SPTM [16]	69.02	60.08	48.27	79.49	65.97	<b>62.52</b>	<b>53.25</b>	50.79
SPTM (epoch 30) [16]	60.16	50.27	39.34	75.46	58.12	54.06	43.92	46.39
PCL [57]	64.75	57.30	40.99	0.04	62.80	58.42	46.96	13.46
VLAD [8], [9]	37.31	27.89	10.53	0.01	21.23	16.92	8.78	0.01
TF-VPR (Ours)	<b>71.94</b>	<b>63.89</b>	<b>52.56</b>	<b>83.34</b>	<b>66.16</b>	62.05	52.49	<b>51.19</b>
TF-VPR (Ours) (epoch 30)	70.97	62.61	50.99	80.79	64.18	60.09	51.44	49.33
NetVLAD [12]	100.00	100.00	100.00	86.38	100.00	100.00	99.99	54.45

clusters for each category, which is not suitable to represent a continuous feature in vision-based SLAM problems. Similarly, VLAD performs poorly when the input resolution is low and the output dimension is small. Moreover, we test the conventional visual SLAM system, like OpenVSLAM [59]. However, OpenVSLAM easily loses track of odometry. A total of 17.75% of the frames are lost during the tracking process. OpenVSLAM builds a disjoint topology graph while tracking odometry, and the recall rate is 54.98% versus 96.23% for TF-VPR. As a result of the poor performance, we do not use OpenVSLAM as a benchmark.

#### D. Experiments on NYU-VPR-360 dataset

**NYU-VPR-360 dataset.** There are several VPR datasets with panoramic images [50], [60], yet few of them have repeated visits to the same place from a variety of angles. To show the ability of our method in retrieving images of different headings, we proposed the NYU-VPR-360 dataset captured by Gopro MAX (a dual-lens 360° camera with GPS recording), which is composed of sequentially collected panoramic RGB images of street views in New York City. The GoPro camera was mounted on the top of the driving vehicle. We utilize the GPS readings of the camera to provide the ground truth of spatial neighborhoods. Note that we select the panoramic images from the whole video to make them synchronized with GPS. The dataset is composed of two driving trajectories, covering an area of approximately  $80,000m^2$ . There are over 15,000 images of  $3840 \times 1920$  pixels in the dataset with their corresponding locations for each scene. Most junctions have at least two types of actions with different driving directions, with the exception of a few intersections that are for traffic reasons.



Fig. 10: Qualitative VPR results on NYU-VPR-360 dataset. The upper part shows an example where TF-VPR outperforms SPTM, and the lower part shows a challenging example in the dataset where only the top-1 retrieval of TF-VPR and VLAD is correct. Green and red respectively indicate true and false positives.

**Baseline methods.** Following IV-C, we use SPTM [16], NetVLAD [12], VLAD [8], [9], and PCL [57] as baselines.

**Implementation details.** The images are resized to  $128 \times 64$  pixels. We set  $n = 10$  and  $u = 5$  as described in Section III-B. For scene 1 and scene 2, based on different sampling rates of the sensors, for each query, we respectively exclude its closest 30 and 100 temporal neighbors from the top-N retrievals as explained in IV-A.

**Comparison with baselines.** The edge of our method is more distinguishable on NYU-VPR-360 dataset as proven by the qualitative results in Fig. 10. As shown in Fig. 6, there is an improvement in the recall rate using TF-VPR. Furthermore, as shown in Table III, TF-VPR surpasses other baselines in recall rate and heading diversity in scene 1 by about 2% and 4% respectively. Furthermore, performance in scene 2 does not improve because there are no spatial positives from different headings in scene 2. More importantly, the performance gap between TF-VPR and other baselines becomes larger over epochs. As shown in Fig. 9, the recall@10 of TF-VPR outperforms the baselines by approximately 8%-10% at epoch 30 as discussed in IV-C.

**Dynamic KNN mechanism.** The distinction between the K-nearest-neighbor specification and the dynamic KNN described in Section III-D is sharper in our real-world experiment. This proves that the dynamic KNN is a better mechanism for selecting feature neighborhoods because its flexibility allows the model to find an adequate number of neighbors for each location in the dataset.

## V. CONCLUSION

We propose TF-VPR as a self-supervised auto-labeling method for determining the unknown spatial neighbors from the fixed temporal neighbors and learnable feature neighbors. Extensive experiments show that TF-VPR not only improves the recall rate over the existing method but also can retrieve spatial positives with more diverse viewpoints on various

datasets. TF-VPR enables easier use of VPR in real-world robotics and computer vision applications, and can be applied to most existing deep-learning-based VPR methods.

**Acknowledgment.** This work is supported by NSF grants under CMMI-1932187, CNS-2121391, and EEC-2036870.

## REFERENCES

- [1] S. Lowry, *et al.*, “Visual place recognition: A survey,” *T-RO*, 2015.
- [2] E. Brachmann and C. Rother, “Visual camera re-localization from RGB and RGB-D images using DSAC,” *TPAMI*, 2021.
- [3] A. Angeli, S. Doncieux, J.-A. Meyer, and D. Filliat, “Real-time visual loop-closure detection,” in *2008 ICRA*, 2008.
- [4] F. Radenović, A. Iscen, G. Tolias, Y. Avrithis, and O. Chum, “Revisiting oxford and paris: Large-scale image retrieval benchmarking,” in *CVPR*, 2018.
- [5] M. Zaffar, *et al.*, “VPR-Bench: An open-source visual place recognition evaluation framework with quantifiable viewpoint and appearance change,” *IJCV*, 2021.
- [6] D. Sheng, *et al.*, “NYU-VPR: Long-term visual place recognition benchmark with view direction and data anonymization influences,” in *IROS*, 2021.
- [7] D. G. Lowe, “Object recognition from local scale-invariant features,” in *ICCV*, 1999.
- [8] H. Jégou, M. Douze, C. Schmid, and P. Pérez, “Aggregating local descriptors into a compact image representation,” in *CVPR*, 2010.
- [9] R. Arandjelovic and A. Zisserman, “All about vlad,” in *CVPR*, June 2013.
- [10] P.-E. Sarlin, C. Cadena, R. Siegwart, and M. Dymczyk, “From coarse to fine: Robust hierarchical localization at large scale,” in *CVPR*, 2019.
- [11] Z. Chen, *et al.*, “Deep learning features at scale for visual place recognition,” in *ICRA*, 2017.
- [12] R. Arandjelovic, P. Gronat, A. Torii, T. Pajdla, and J. Sivic, “Netvlad: Cnn architecture for weakly supervised place recognition,” in *CVPR*, June 2016.
- [13] S. Garg, M. Vankadari, and M. Milford, “Seqmatchnet: Contrastive learning with sequence matching for place recognition & relocalization,” in *CoRL*. PMLR, 2022.
- [14] A. Forechi, A. F. De Souza, C. Badue, and T. Oliveira-Santos, “Sequential appearance-based global localization using an ensemble of knn-dtw classifiers,” in *IJCNN*, 2016.
- [15] O. Vysotska and C. Stachniss, “Lazy data association for image sequences matching under substantial appearance changes,” *RA-L*, 2015.
- [16] N. Savinov, A. Dosovitskiy, and V. Koltun, “Semi-parametric topological memory for navigation,” in *ICLR*, 2018.
- [17] S. E. Reed, H. Lee, D. Anguelov, C. Szegedy, D. Erhan, and A. Rabinovich, “Training deep neural networks on noisy labels with bootstrapping,” in *ICLR (Workshop)*, 2015.
- [18] M. Cummins and P. Newman, “FAB-MAP: Probabilistic localization and mapping in the space of appearance,” *IJRR*, 2008.
- [19] N. Cummins, Mark and Paul, “Appearance-only SLAM at large scale with FAB-MAP 2.0,” *IJRR*, 2011.
- [20] M. J. Milford, G. F. Wyeth, and D. Prasser, “Ratslam: a hippocampal model for simultaneous localization and mapping,” in *ICRA*, 2004.
- [21] D. Galvez-Lopez and J. D. Tardos, “Real-time loop detection with bags of binary words,” in *IROS*, 2011.
- [22] M. J. Milford and G. F. Wyeth, “Seqslam: Visual route-based navigation for sunny summer days and stormy winter nights,” in *ICRA*, 2012.
- [23] G. Costante, T. A. Ciarfuglia, P. Valigi, and E. Ricci, “A transfer learning approach for multi-cue semantic place recognition,” in *IROS*, 2013.
- [24] N. Sünderhauf, *et al.*, “Place recognition with convnet landmarks: Viewpoint-robust, condition-robust, training-free,” in *Robotics: Science and Systems XI*. Robotics: Science and Systems Conference, 2015.
- [25] M. Lopez-Antequera, R. Gomez-Ojeda, N. Petkov, and J. Gonzalez-Jimenez, “Appearance-invariant place recognition by discriminatively training a convolutional neural network,” *Pattern Recognition Letters*, 2017.
- [26] T. Naseer, G. L. Oliveira, T. Brox, and W. Burgard, “Semantics-aware visual localization under challenging perceptual conditions,” in *ICRA*, 2017.
- [27] S. Garg, N. Sünderhauf, and M. Milford, “Lost? appearance-invariant place recognition for opposite viewpoints using visual semantics,” *arXiv preprint arXiv:1804.05526*, June 2018.
- [28] C. Choy, J. Park, and V. Koltun, “Fully convolutional geometric features,” in *ICCV*, 2019.
- [29] H. Deng, T. Birdal, and S. Ilic, “Ppfnet: Global context aware local features for robust 3D point matching,” in *CVPR*, 2018.
- [30] M. A. Uy and G. H. Lee, “PointNetVLAD: Deep point cloud based retrieval for large-scale place recognition,” in *CVPR*, 2018.
- [31] Z. Liu, *et al.*, “Lpd-net: 3d point cloud learning for large-scale place recognition and environment analysis,” in *ICCV*, 2019.
- [32] X. Chen, *et al.*, “Overlapnet: Loop closing for lidar-based slam,” in *Robotics: Science and Systems*, 2020.
- [33] K. Cai, B. Wang, and C. X. Lu, “Autoplace: Robust place recognition with low-cost single-chip automotive radar,” in *ICRA*, 2022.
- [34] S. Lowry and M. J. Milford, “Supervised and unsupervised linear learning techniques for visual place recognition in changing environments,” *T-RO*, 2016.
- [35] N. Merrill and G. Huang, “Lightweight unsupervised deep loop closure,” in *Robotics: Science and Systems*, 2018.
- [36] X. Gao and T. Zhang, “Unsupervised learning to detect loops using deep neural networks for visual SLAM system,” *Autonomous robots*, 2017.
- [37] O. Kwon, N. Kim, Y. Choi, H. Yoo, J. Park, and S. Oh, “Visual graph memory with unsupervised representation for visual navigation,” in *ICCV*, 2021.
- [38] N. Natarajan, I. S. Dhillon, P. K. Ravikumar, and A. Tewari, “Learning with noisy labels,” *NeurIPS*, 2013.
- [39] H. Song, M. Kim, D. Park, Y. Shin, and J.-G. Lee, “Learning from noisy labels with deep neural networks: A survey,” *TNNLS*, 2022.
- [40] Z. Yu, *et al.*, “Simultaneous edge alignment and learning,” in *ECCV*, 2018.
- [41] G. Patrini, A. Rozza, A. Krishna Menon, R. Nock, and L. Qu, “Making deep neural networks robust to label noise: A loss correction approach,” in *CVPR*, 2017.
- [42] D.-H. Lee *et al.*, “Pseudo-label: The simple and efficient semi-supervised learning method for deep neural networks,” in *ICML*, 2013.
- [43] Y. Zou, Z. Yu, B. Kumar, and J. Wang, “Unsupervised domain adaptation for semantic segmentation via class-balanced self-training,” in *ECCV*, 2018.
- [44] Y. Zou, Z. Yu, X. Liu, B. Kumar, and J. Wang, “Confidence regularized self-training,” in *ICCV*, 2019.
- [45] K. He, H. Fan, Y. Wu, S. Xie, and R. Girshick, “Momentum contrast for unsupervised visual representation learning,” in *CVPR*, 2020.
- [46] A. v. d. Oord, Y. Li, and O. Vinyals, “Representation learning with contrastive predictive coding,” *arXiv preprint arXiv:1807.03748*, 2018.
- [47] Y. Tian, D. Krishnan, and P. Isola, “Contrastive multiview coding,” in *ECCV*. Springer, 2020.
- [48] Y. Tian, C. Sun, B. Poole, D. Krishnan, C. Schmid, and P. Isola, “What makes for good views for contrastive learning?” *NeurIPS*, 2020.
- [49] R. Arandjelović and A. Zisserman, “Visual vocabulary with a semantic twist,” in *ACCV*. Springer, 2014.
- [50] A. Torii, R. Arandjelovic, J. Sivic, M. Okutomi, and T. Pajdla, “24/7 place recognition by view synthesis,” in *CVPR*, 2015.
- [51] L. Ding and C. Feng, “Deepmapping: Unsupervised map estimation from multiple point clouds,” in *CVPR*, 2019.
- [52] P. C. Ng and S. Henikoff, “Sift: Predicting amino acid changes that affect protein function,” *Nucleic acids research*, 2003.
- [53] P. Achlioptas, O. Diamanti, I. Mitliagkas, and L. Guibas, “Learning representations and generative models for 3d point clouds,” in *ICML*. PMLR, 2018.
- [54] M. Savva, *et al.*, “Habitat: A platform for embodied AI research,” in *ICCV*, 2019.
- [55] A. Paszke, *et al.*, “Automatic differentiation in pytorch,” *arXiv preprint arXiv:2010.07922*, 2017.
- [56] D. P. Kingma and J. Ba, “Adam: A method for stochastic optimization,” in *ICLR*, 2015.
- [57] J. Li, P. Zhou, C. Xiong, and S. C. Hoi, “Prototypical contrastive learning of unsupervised representations,” in *ICLR*, 2021.
- [58] F. Xia, A. R. Zamir, Z.-Y. He, A. Sax, J. Malik, and S. Savarese, “Gibson env: real-world perception for embodied agents,” in *CVPR*, 2018.
- [59] S. Sumikura, M. Shibuya, and K. Sakurada, “Openvslam: A versatile visual slam framework,” in *ACM Multimedia*, 2019.
- [60] A. Torii, J. Sivic, T. Pajdla, and M. Okutomi, “Visual place recognition with repetitive structures,” in *CVPR*, 2013.